Examining the relationship between morphological variation and modeled broadband scattering responses of reef-associated fishes from the Southeast United States

[*1]Kevin M. Boswell, [2,3]Geir Pedersen, [4]J. Christopher Taylor, [1]Savannah LaBua, [5]William F. Patterson, III.

[1]Florida International University, Department of Biological Sciences, Marine Science Program, North Miami, Florida, 33181. USA.

[2]NORCE Norwegian Research Centre AS, Fantoftvegen 38, 5072 Bergen, Norway

[3]Institute of Marine Research, P.O Box 1870 Nordnes, Bergen, Norway

[4]National Centers for Coastal Ocean Science, NOAA Beaufort Laboratory, 101 Pivers Island Rd., Beaufort, North Carolina 21516, USA.

[5]Fisheries and Aquatic Sciences, University of Florida, 7922 NW 71st Street, Gainesville, Florida 32608, USA

*Corresponding Author: Kevin M. Boswell, Florida International University, 3000 NE 151st St., MSB359, North Miami, FL 33181. Kevin.boswell@fiu.edu

Examining the relationship between morphological variation and modeled broadband scattering responses of reef-associated fishes from the Southeast United States

[*1]Kevin M. Boswell, [2,3]Geir Pedersen, [4]J. Christopher Taylor, [1]Savannah LaBua, [5]William F. Patterson, III.

[1]Florida International University, Department of Biological Sciences, Marine Science Program, North Miami, Florida, 33181. USA.

[2]NORCE Norwegian Research Centre AS, Fantoftvegen 38, 5072 Bergen, Norway

[3]Institute of Marine Research, P.O Box 1870 Nordnes, Bergen, Norway

[4]National Centers for Coastal Ocean Science, NOAA Beaufort Laboratory, 101 Pivers Island Rd., Beaufort, North Carolina 21516, USA.

[5]Fisheries and Aquatic Sciences, University of Florida, 7922 NW 71st Street, Gainesville, Florida 32608, USA

*Corresponding Author: Kevin M. Boswell, Florida International University, 3000 NE 151st St., MSB359, North Miami, FL 33181. Kevin.boswell@fiu.edu

Abstract

Non-lethal methods are sought to provide indices or measure of absolute abundance to fit fishery stock assessment models, including those computed for reef fishes. Calibrated scientific echosounders provide the foundation for stock assessments in low-diversity ecosystems but are hampered by complicated target strength responses in high diversity systems like coral and rocky reefs. Newly available broadband echosounders present advantages over narrowband predecessors including increased spatial resolution, increased signal to noise and spectral resolution; however, a better understanding of the sound scattering properties is necessary for operational use in surveys of diverse reef fish assemblages. To gain insight into the feasibility of implementing broadband techniques, we first model the frequency dependent backscatter of ecologically and commercially important species; results will aid our understanding of the backscattering as well as provide a supporting dataset to develop algorithms for classification of species/functional groups. Computed-tomography (CT) scans were performed on 149 individuals across reef fish species from the northeastern Gulf of Mexico to generate three-dimensional swim bladder models for estimation of morphometrics to input into numerical scattering models. Principal component analysis of the swim bladder morphology indicated significant variation among species; however, closely related species (confamilials) were not different. We employed boundary element method modeling to examine the frequency-dependent backscatter responses across a range of fish orientations (+/- 45^{o}). Comparisons of frequency-dependent backscatter revealed strongest similarities between closely related species and greatest differences between more distantly related species or species groups. Patterns in the spectra have the potential to be used to classify targets toward species (or species group) for estimates of density from marine ecosystem acoustic surveys. Given that broadband echosounders are not yet commonplace, and

41 many surveys in the region utilize narrowband echosounders, we also developed narrowband
42 target strength – length relationships for six of the reef fish species with model fits ranging
43 widely (r^2 = 0.05 to 0.93). The potential utility of broadband echosounders to enhance ecosystem
44 studies, or to develop fisheries-independent indices of abundance for use in stock assessment is
45 discussed.

46 **Keywords**: Boundary Element Method, broadband acoustics, reef fish, target strength, swim
47 bladder.

48 **Introduction**

49 Reef fishes are ecologically significant members of rocky and coral reef ecosystems and
50 support economically important fisheries in US waters of the Gulf of Mexico (GOM), Atlantic
51 Ocean, and Caribbean Sea. Despite their ecological and economic importance, many reef fishes
52 in the southeastern US (SEUS) are estimated to be fully exploited or overfished and regional
53 management is contentious given the diversity of commercial and recreational user groups that
54 participate in SEUS reef fisheries (Die et al. 1988; Johnston et al. 2010; Cowan et al. 2011). In
55 the northern GOM (nGOM), large-scale events such as red tides, the Deepwater Horizon oil spill
56 (DWH), or the proliferation of invasive red lionfish (*Pterois volitans*/*mile*s complex), also have
57 complicated assessments and management of SEUS reef fish stocks by depletion or causing
58 shifts in community structure.

59 Stock assessments for exploited reef fishes in the SEUS typically have relied on fishery-
60 dependent data (derived from commercial fisheries harvest data) not only to estimate the catch-
61 at-age of fishery landings, but also to compute population indices and trends over time. Fishery-
62 dependent data may be biased by fishery selectivity, shifting fishery regulations over time, or
63 hyperstability of reef fish catch rates. Therefore, fishery-dependent data are complimented in

most assessments with fishery-independent (derived from research surveys at sea) time series to track abundance of particular life stages across time (Hilborn and Walters 2013). These data often prove to be invaluable given survey designs are stratified, randomized and follow standardized methodologies, thus accounting for gear selectivity and providing unbiased parameter estimates of target species. Furthermore, fishery-independent methods can be employed to examine ecological questions and to develop habitat or region-specific baselines in the event of large-scale anthropogenic stressors.

The physical structure of reefs, whether they are natural or artificial, precludes the usage of many extractive gear types, such as trawls or gillnets, to conduct fishery-independent sampling. Other catch-based methods, such as handline or bottom longline sampling, can be deployed for fishery-independent sampling, but extractive gears are counterproductive for imperiled or overfished stocks. In such cases, non-extractive gears, such as video-based sampling provide less invasive methods (Bacheler *et al*. 2013; Campbell *et al*. 2015). Acoustic surveys are a primary assessment method in several ecosystems, best exemplified by low diversity or high abundance of aggregating or schooling species (e.g., Celtic Sea, Atlantic herring; Barents Sea, demersal fish; Northwest Pacific Ocean, Pacific hake; Cook Strait, hoki). Challenges arise when attempting to employ acoustic methods in reef ecosystems with diverse fish assemblages since species may have backscatter responses that are similar in their frequency-dependent patterns, thus inhibiting the potential for using backscatter as a discriminating attribute. Moreover, proximity to reef structure can also affect the ability to detect fish biomass with acoustics (Gledhill et al. 1996; Rudershausen et al. 2010).

New commercially available broadband echosounders are showing promise in the ability to enhance the data collected across continuous acoustic spectra (i.e., 30- 200kHz). There are

several advantages that broadband techniques offer over traditional narrowband echosounders with limited bandwidth (~1-5 kHz); namely an increase in range resolution permitting better separation among targets and between targets and the seafloor, characterization of the acoustic backscatter of targets across a frequency spectrum and an increase in signal to noise (Chu and Stanton, 1998; Ehrenberg and Torkelson, 2000; Demer et al. 2017; Lavery et al. 2017; Bassett et al. 2017). Among these advantages, the potential exists to interpret species-specific signatures of target backscatter due to variation in the morphology of gas-filled swim bladders among species.

Broadband echosounders transmit and receive acoustic signals along a continuous frequency spectrum. Previous work using low- (1.7-6 kHz) to mid-frequency (6-17 kHz) echosounders was mostly focused on the discriminating power of using the resonating frequency to separate taxa of marine organisms (Stanton et al. 2010, 2012; Benoit-Bird and Lawson 2016). Less work has been devoted to understanding the variation in frequency-dependent backscatter for diverse assemblages of reef fishes at the higher frequency ranges (>18 kHz), and in particular for species common to the SEUS, GOM and Caribbean regions (Johnston et al. 2006). Results of work by Au and Benoit-Bird (2003) demonstrate the potential for discriminating among similar reef species using broadband echosounders by exploiting the variation in morphology and orientation of gas-filled swimbladders which contribute to variation in the waveform of frequency-dependent backscatter.

Theoretical models of acoustic backscatter are commonly used to examine the predicted backscatter of dominant species that have economic or ecological importance (reviewed by Jech et al. 2016). Generally, these models compute the theoretical acoustic backscatter attributable to the swim bladders, accounting for variation in the physical dimensions, shape and orientation of, the swimbladder (e.g. Jech et al., 2015 and Macaulay et al., 2013). We implemented a numerical

method (Boundary Element Method; BEM) so as not to be limited to prolate spheroids or other simplified shapes, and to be able to calculate for any angle of incidence and frequency or the product of acoustic wavenumber and dimensions of the swim bladder model. The steep slope of the swim bladder of many specimens relative to the body is an additional complication, favoring the use of general numerical approaches over methods employing Kirchoff approximation (Foote and Francis 2002; Macaulay *et al*., 2013).

We examined the species-specific scattering spectra of predominant reef fishes found on GOM reefs to determine the theoretical feasibility of using broadband approaches for species or species group discrimination. An analysis of the morphometry of the swim bladders and output from theoretical models of acoustic backscatter were compared among species to quantify frequency and angle dependencies in scattering properties of selected species. Lastly, we investigate the potential of exploiting target strength frequency responses as signatures to discriminate among species and provide species- or guild-specific estimates of fish density using echosounder surveys of reef systems.

Methods

Fish collection

Fish were collected with baited hook and line over coastal reefs during daylight hours (<30 m depth) south of Orange Beach, Alabama, USA aboard a for-hire recreational fishing vessel during August-September 2017. Captured fish were slowly retrieved and placed in an aerated holding tank on board the fishing vessel. Once back at the dock, fish were transported to the University of South Alabama Health University Hospital imaging facility in aerated tanks. Prior

to imaging, fish were anesthetized in an ice slurry and then placed on the imaging platform.

Computed Tomographic Imaging

Morphological characteristics of reef fish were investigated through the quantitative use of computed tomography (CT) scans on 149 individuals among nine nGOM reef fish species, including three grunt species (Family Haemulidae): blue striped grunt (BSG), *Haemulon sciurus*, white grunt (WG), *Haemulon plumieri*, and tomtate (Tom), *Haemulon aurolineatum*; two snapper species (Family Lutjanidae): red snapper (RS), *Lutjanus campechanus*, and vermilion snapper (VS), *Rhomboplites aurorubens*; and, four additional species: bank sea bass (BSB), *Centropristis striata*; gray triggerfish (GT), *Balistes capriscus*; hogfish (Hog), *Lachnolaimus maximus*; red band parrotfish (RBP), *Sparisoma aurofrenatum* (Table 1). The fish species examined are numerically abundant and ecologically significant in this region of the northeastern Gulf of Mexico, with most also targeted in recreational or commercial fisheries. Blue striped grunt, hogfish, and red band parrotfish are predominant members of the reef fish community in south Florida waters, while gray triggerfish, red snapper, tomtate, vermilion snapper, and white grunt have tropical to subtropical distributions in US Atlantic and Gulf of Mexico waters. The size ranges of fishes sampled and scanned for swim bladder morphology are typical of adult size ranges encountered in this region of the Gulf of Mexico.

Conducting CT scans is an efficient means of acquiring high-resolution three-dimensional models of fish, including the internal musculature, skeletal components and swim bladder. This method is superior to traditional bi-planar x-ray imagery as the curvature and fine-scale structure of the bladder can be discerned and modeled. Fish were scanned along the longitudinal axis and resulted in a series of cross-sectional slices through the body yielding detailed images of the

internal structure of each individual that could be quantified through image processing. Images were collected with a Philips Brilliance 16P machine set to collect images at 1 mm thickness, 0.5 mm interslice spacing, 120 kVp, data collection diameter of 500 mm, reconstruction diameter of 250 mm, exposure time of 381 ms and filter type B. Three dimensional models of bladders were derived for each individual, permitting examination of species-specific morphological variation (Fig. 1) and parameterizing target strength models for each individual.

Images were imported into AMIRA (v6.2.0) to facilitate the bladder measurement procedure. Bladder shapes were extracted by thresholding and classifying each voxel through the segmentation interface using a masking range in AMIRA from -1024 to -100; the wide range was a function of variation across species. The processing of each bladder within AMIRA yielded outputs of morphological metrics for each fish (Table 1). For each individual the following were measured: total length (mm); fish height (mm) was measured as the greatest vertical distance along the transverse plane; fish thickness (mm) was measured as the greatest lateral distance across the transverse plane; bladder length (mm) and bladder height (mm) were both measured similarly to fish length and height; bladder angle (the angle that the bladder sits within the body) of the fish, normal to the dorsal plane, was measured as the distance between a coordinate at the posterior and anterior points of the bladder (Fig. 2). For each individual, a three-dimensional stereolithography (STL) file was created and imported into Autodesk Fusion 360 (v2.0.30330) for further processing. Mesh face counts were reduced to smooth the models and remove deformities (e.g., anomalies generated during image segmentation and processing). Models of each bladder were then adjsuted for proper oriented using Autodesk Netfabb Basic (v2017.2) such that the dorsal side of the bladder was oriented towards the -X plane and the point of contact between the bladder and vertebral column oriented towards the -Y plane. Bladders

were rescaled in Blender (v2.78). Models were imported into Netgen (v5.3) to generate a final wire mesh model for acoustic backscatter simulations using the BEM, described below. Lastly, each wire mesh was imported into GMSH (version 2.7.0) and converted from STL format into the msh format required for BEM code.

Morphometric Analysis

A principal component analysis (PCA) was conducted on swim bladder morphometrics to reduce dimensionality of the data and address collinearity among variables while allowing for comparisons of the shape and orientation among species. The metrics were manually measured from each CT scan (Table 1), in addition to two derived morphological indices, were included in the PCA: the ratios of the swim bladder length (mm) to fish length (mm) and swim bladder height (mm) to fish height (mm). The first two components (explaining greater than 98% of the total variance) were retained and further used to describe the variation in swim bladder morphology among the species sampled.

Backscatter modeling and analysis

Frequency-dependent wire-meshes were generated (Netgen v5.3) for the swim bladder models at the following resolution 30-50 kHz (0.0015 mm), 52-100 kHz (0.00075 mm), 102-150 kHz (0.0005 mm), and 152-200 kHz (0.000375 mm), always exceeding 10 nodes per wavelength across the frequency band. Variable mesh resolution was required to reduce the computational resources needed at the higher frequencies where high-density meshes exceeded the computational capabilities of the High-Performance Computing Cluster at Florida International University (30 Cores, high-memory nodes).

The backscattered target strength ($TS = 10log_{10}(\sigma_{bs})$) [dB re 1 m^2], where (σ_{bs}, [m^2])

represents the cross-sectional backscatter from an individual (MacLennan 1990), was calculated from each three-dimensional CT-model. *TS* was computed from 30-200 kHz at 2 kHz intervals and over a range of tilt angles from -45 to +45 degrees in 2 degree increments, where 0 degrees represents the dorsal orientation. This range in orientation was included to examine the *TS* variation relative to how a fish might be distributed within the water column (Gastauer et al. 2016).

An open-source library for the solution of boundary integral equations for Laplace, Helmholtz and Maxwell problems in three dimensions (BEM++ v 2.0.3; Śmigaj et al., 2015) was used to calculate acoustic backscattering from the digitized swimbladders. A combined direct formulation was utilized (Chandler-Wilde, 2012) with pressure release boundary conditions. Fast solution of the boundary-element problems was achieved through the implementation of the adaptive cross approximation (ACA) algorithm.

The implementation was verified by calculating backscattering from spheroids and comparison with analytic methods. Convergence tests were performed with varying mesh densities prior to the simulations. BEM has previously been used successfully to model backscatter by swimbladders and swim bladder like shapes (e.g. Francis and Foote, 2003; Okumura et al., 2003).

Target strength and fish length relationships

Relationships between target strength and total fish length (*TL*, cm) were examined for each species at the nominal narrowband center frequencies commonly applied in fisheries surveys (38, 70, 120, 200 kHz) with the nlme package (R, v3.5). Regression analyses were developed for each species where there were four or greater number of individuals. Target strength to fish length

relationships were modelled with the equation $TS = m\ log_{10}\ TL + b$. Two models were fit to the data. In the first model, the slope (m) and y-intercept (b_0) parameters were estimated with standard regression techniques (following Nakken and Olsen, 1977). In the second model, the standard form in which the slope parameter (m) was fixed at 20 and the intercept (b_{20}) was estimated, given that σ_{bs} is proportional to the square of fish length (Love 1977; Foote 1979), as discussed below.

Spectral scattering responses

Length normalized target strength was computed for each swim bladder across the range of angles and frequencies with the equation $nTS = 10log_{10}(\sigma_{bs}/L^2)$ [dB re 1 m^2], where σ_{bs} is measured at any given angle and frequency, and L [cm] is bladder length (Love 1977, Macaulay et al. 2013). The resulting matrix was used to derive angle averaged (+/-10 degree) backscatter responses representative of each species. Global kernel density distributions of target strength were computed from all individuals within each species using an individual's averaged response between +/- 10 degrees from normal (dorsal) incidence using the *ksdensity* function (Matlab v9.5, Mathworks, Inc.) to avoid forcing assumptions about underlying *TS* distributions for each species.

Results

Species specific variability in swim bladder morphology

Significant variation among the morphological variables was observed, indicating that the dimensions of both the fish and swim bladder were important in yielding separation among species within the principal component space (Table 1). In addition to size, the angle of the bladder (relative to the horizontal orientation) was significant in separating among species (Fig.

243 3). The PCA describing the morphological characteristics of fish and swim bladders indicated
244 high covariance among the selected variables. Variables with a loading greater than 0.50 were
245 considered to contribute to a PC. The first PC accounted for the majority of the variation
246 explained among variables (65.1%), with PC2 accounting for approximately 34% of the variance
247 across the modeled individuals. Strong allometry existed overall between fish length and fish
248 swim bladder length, indicating a positive linear relationship (Fig. 4; Table 2). Among the
249 species modeled, regression models were significant, but the fits were variable (p<0.05; Table 2),
250 ranging from a relatively poor fit for gray triggerfish (R^2=0.38) to blue stripe grunt with a
251 relatively strong fit (R^2 = 0.95).

252 *Species TS response across frequencies and angles*

253 The target strength-frequency spectra derived from the BEM models illustrate wide variation
254 across species, though some generalities were observed (Fig. 5). For example, the three grunt
255 species (Family Haemulidae) displayed consistently similar responses across frequencies and
256 orientation, while the lutjanids, red snapper and vermillion snapper, were conspicuously
257 dissimilar. Peaks in the scattering responses were observed among most examples where the
258 incident angles were approximately between -10 to -30 degrees, representing angles where the
259 cross-sectional area of the bladder tended to be oriented horizontally, and orthogonal to the
260 transmitted pulse. In species with more uniform shapes (e.g., bank sea bass and gray triggerfish),
261 the *TS* response was much more variable across the same orientation ranges. (Fig. 5). Qualitative
262 examination of the angle-averaged (-10: +10 degree) normalized σ_{bs} frequency response
263 indicated wide variation among species in the magnitude of backscatter, with profiles among
264 species being divergent across the nominal center frequencies of common echosounders (38, 70,
265 120, 200 kHz) (Fig. 6). The bladder length-normalized frequency spectra for nearly half the

266 species lacked obvious spectral features (blue striped grunt, red band parrotfish, vermillion
267 snapper, tomtate, white grunt) (Fig. 6). In contrast, the bank sea bass, gray triggerfish, hogfish,
268 and red snapper all showed more complex frequency-dependent backscatter across the modeled
269 frequencies (Fig. 6). When considering the nominal frequencies sampled, gray triggerfish had the
270 greatest length-normalized backscatter (σ_{bs}) (0.0702 m^2 at 154 kHz), while vermillion snapper
271 (0.0101 m^2 at 74 kHz) and red band parrotfish (0.0043 m^2 at 123 kHz) were the lowest (Fig. 6).

272 Linear relationships between *TS* and $\log_{10}$ *TL* were computed for six of the nine modeled
273 species (Table 3) across the four discrete frequencies (38, 70, 120, and 200 kHz). In general,
274 adopting the standard b_{20} *TS-TL* form resulted in poorer fits across the modeled species in
275 comparison to model-fitted slopes (Table 3). Across most frequencies red snapper had the
276 greatest b_{20} of modeled species (-64.5 dB) and occurred at 70 kHz; while vermillion snapper had
277 consistently lower intercepts (b_0 and b_{20}) than others by greater than 3 dB and was the only
278 species for which the intercepts declined with increasing frequency (Fig. 7).

279 Examination of the kernel density distributions of target strength indicate wide variability
280 among the species examined (Fig. 8). The overall kernel density distribution of vermilion
281 snapper *TS* was the lowest of all modeled species with slight overlap in the upper end of the
282 distribution with the haemulids. Within the Haemulidae, the tomtate exhibited a very narrow and
283 characteristic *TS* distribution relative to other haemulids and other species. The gray triggerfish
284 and red snapper were characterized by greater *TS* which generally did not overlap with the other
285 species (Fig. 8).

286 **Discussion**

287 The CT scans revealed wide variation in the swim bladder and body morphology in addition

288 to the orientation of the bladder within the body, which was largely reflected in the variation in
289 backscatter among taxa. While the three species in the family haemulidae (blue striped grunt,
290 tomtate, and white grunt) displayed similarities in both morphology and predicted backscatter,
291 the two lutjanid species (red snapper and vermillion snapper) were quite different in both
292 morphological characteristics and backscatter responses. Others have demonstrated variation in
293 shape parameters among closely related species, and among lutjanids in particular; however, as
294 reported by Benoit-Bird et al. (2003), the acoustic properties did not vary significantly among
295 closely related species.

296 Understanding the acoustic backscattering response (*TS*) from fish is vital for absolute
297 abundance estimation and acoustic species discrimination. *TS* is usually examined through a
298 great number of measurements from a combination of *ex situ* (immobilized or caged fish) and *in*
299 *situ* free-swimming measurements. Each method has its own challenges: fish might not exhibit
300 natural behavior during *ex situ* experiments, whereas obtaining sufficient measurements,
301 confirming species identification and physically sampling fish *in situ* can be difficult. Due to
302 these limitations, modelling plays a key role to increase the number of samples, interpret
303 experimental data, and understand the underlying physical processes. As previous studies have
304 demonstrated, despite the absence of complementary *in situ* backscatter data, models derived
305 from simulated backscatter provide valuable opportunities to investigate species-specific
306 patterns. Importantly, the *TS-L* relationships provided in this paper are the first for the species in
307 the Gulf of Mexico region and can be used by researchers to begin to investigate the use of
308 multiple frequencies or broadband approaches for discrimination among the species complex
309 during fishery independent surveys. It is largely understood that for fishes with swim bladders,
310 the bladder is the major contributor (~90-95%) to observed acoustic backscattering (Foote

311 1980a; Ona 1990). However, the received amplitudes of backscatter can be mediated by fish size
312 (Love 1977; Simmonds and MacLennan 2005), orientation (Nakken and Olsen 1977; Foote
313 1980b; Benoit-Bird et al. 2003; Hazen and Horne 2003), physiology (Horne 2003) and material
314 properties (Scoulding et al. 2015; Reeder et al. 2004). With respect to the species examined,
315 considerable variation was observed in the morphological properties, and is likely the main
316 contributor to the variation observed in the modeled backscatter. In some cases, this variation
317 resulted in species-specific backscatter responses which may help to distinguish predominant
318 reef fishes on nGOM reefs. For example, gray triggerfish which have a distinctly rounded swim
319 bladder with a steeper bladder angle relative to the more horizontally elongated bladders of other
320 species resulted in a distinctive *TS*-frequency response across incidence angles when compared
321 to other species.

322 While acoustic models do not exist that describe these species specifically, others have
323 performed similar analyses, both via modeling and *in situ* observation, on related species (Au
324 and Benoit-Bird 2003; Benoit-Bird *et al*., 2003; Gastauer *et al*., 2016; 2017a, b). The snapper
325 species that were examined by both Au and Benoit-Bird (2003) and Benoit-Bird *et al*. (2003)
326 displayed considerable variance in both swimbladder morphology and the modeled broadband
327 frequency response across angles. Gastauer *et al*. (2016) examined the *TS* response for a related
328 *Balistidae* species and developed a *TS*-*L* relationship, although from a considerably smaller fish
329 (~26 cm), with a difference in *TS* of approximately 10 dB in comparison to the *TS*-*L* relationship
330 we presented in Table 3. At present, the Gastauer *et al*. (2016, 2017a, b) models are the closest in
331 comparison to the models we present, for Families Lutjanidae and Balistidae, but in both cases
332 the b_{20} intercepts derived in our angle-averaged models were substantially greater, than the range
333 of 5.1 to 8.5 dB for goldband snapper *Pristipomoides multidens* (Gastauer *et al*., 2017) and red

334 emperor *Lutjanus sebae* (Gastauer *et al*., 2016), respectively. Similarly, the model derived for
335 gray triggerfish at 38 kHz had a b_{20} intercept approximately 10 dB greater than the balistids
336 modeled by Gastauer *et al*., (2017a). While the differences are likely explained, by variation in
337 the range of modeled fish lengths and, perhaps, species-specific morphology, they may also be
338 due in part to the different modeling strategies. Specifically, the models employed by Benoit-
339 Bird *et al*., (2003) were based on a prolate spheroid (Furusawa 1988); whereas, Gastauer *et al*.,
340 (2016, 2017a,b) models were based on the Kirchoff-ray mode model (Clay and Horne 1994). In
341 contrast, we developed models using the BEM approach. It should be noted that at present, an
342 important limitation of implementing numerical methods such as BEM is that they are
343 computationally demanding, particularly at high acoustic frequencies. This is because in order to
344 represent an acoustic wave on a discrete grid (the mesh), the mesh elements must be smaller than
345 the wavelength in order to resolve the wave. This of course is expected to become less of an
346 impediment with improvements in processing capacity and efficiency.

347 The dorsal-aspect backscattering response we report across a wide range of incident
348 angles was intended to represent natural tilt distributions of fish swimming near reefs. While the
349 *in situ* orientation of fish is likely variable, the mean and magnitude of tilt angles *in situ* is
350 unknown and has not been extensively studied in these GOM species. Our initial normal tilt
351 distributions assumed orientations between +/- 30 degrees, although this may not include active
352 swimming or other behaviors related to schooling behaviors, feeding, predator evasion,
353 courtship, etc. (Benoit-Bird *et al*., 2003; Lundgren and Nielsen 2008). When examining the
354 frequency-dependent *TS* responses it appears that across most species, perhaps except for gray
355 triggerfish, the peak *TS* amplitude is associated with a -15 to -25 degree tilt, where the swim
356 bladder would be perpendicular to the incident angle of the sound source (i.e., head down),

357 resulting in an increase in the cross-sectional scattering area of the swim bladder from the dorsal
358 perspective. Interestingly, the three haemulids and vermillion snapper were characterized with a
359 consistent frequency response at those angles, while other species displayed much more
360 complexity, likely attributed to finer structural differences in the swim bladder. Additional effort
361 will be required to better understand the true range of tilt angles under natural conditions, and
362 advances in broadband split-beam processing may help acquire empirical data to infer *in situ* tilt
363 distributions.

364 The interest in broadband techniques to aid in the classification and identification of
365 taxonomic groups in aquatic ecosystems has increased recently and will likely continue as
366 advances are developed. Given that the acoustic backscatter is a function of the physical
367 attributes of an ensonified target, the variation we observed suggests that some potential may
368 exist for exploiting increased bandwidth to distinguish among taxa. Not only did we observe
369 variation in the frequency- dependent *TS* responses among species, but the mean *TS* distributions
370 indicate that among the species we examined, some may have characteristic *TS* distributions
371 (Fig. 8). For example, the three haemulids were characteristically clustered with overlapping *TS*
372 distributions from -41 to -46 dB. No other species significantly overlapped with those three.
373 Moreover, vermillion snapper and red snapper, which differ in overall body shape and are
374 relatively distantly related among snapper species (Gold *et al*., 2011; Da Silva *et al*., 2018), were
375 well separated from one another suggesting that in cases where the dominance among these
376 species vary significantly, we may be capable of isolating taxonomic groups. Through an
377 extensive analysis of the frequency-dependent *TS* responses from the species examined here Roa
378 et al. (in review) determined that the following frequencies 36, 70, 90, 140, and 190 kHz, carry
379 the most discrimination information for these species examined in this study.

While this study was focused on deriving the acoustic scattering characteristics of the swim bladder, it is important to consider other sources of uncertainty where model predictions may deviate from empirical measures. For example, we did not consider the contributions of backscatter attributable to the body components other than the swim bladder, which may be important, particularly at greater frequencies (Gastauer *et al*., 2017b; Reeder *et al*., 2004; Nesse *et al*., 2009; Forland *et al*., 2014a,b). Additionally, given that these fish can be distributed across a range of depths, further study is needed to understand the effects of depth on swimbladder shape and morphology and future models should account for pressure effects in *TS* modeling. While the fish we examined were from moderate depths where barotrauma was not a factor, these species are commonly found in waters greater than 60 m and additional effort will be needed to update these models to compensate for the effects of water depth. Pressure may exert a non-homogeneous change in swim bladder morphology for each species, an observation that will be challenging to document, but critical for understanding *in situ* variation in broadband *TS* responses (Francis and Foote 2003).

Conclusions

In situ measures are preferred over modeling output alone for examining the acoustic backscatter properties of fishes and the ability to utilize frequency spectra to distinguish species associated with reefs. However, when planning for surveys and in the absence of empirical measures, the modeling responses can be very useful to describe expected frequency-dependent backscatter based on species-specific morphology (Horne *et al*., 2000; Fässler *et al*. 2013; Scoulding *et al*., 2015; Gastauer *et al*., 2016) to inform survey plans and selection of the proper

frequencies for use within a given ecosystem. Broadband methods for discriminating and classifying among taxa have been the focus of many studies (Holliday, 1977; Stanton *et al*., 1998, 2012; Ross *et al*., 2013; Jech *et al*., 2017, Zakharia *et al*. 1996, Reeder *et al*. 2004) as well as offering high resolution insight into the anatomy of fish targets and examining the relative contributions of the scattering features (e.g., separating bladder from head and tail, etc.). While these results offer important insight into the potential differences among species, future effort should be focused on deriving *in situ* measures of *TS* and evaluate the agreement with modeled output (Pena and Foote 2008; Gastauer et al. 2016).

The ability to implement these model results presented herein, and ultimately incorporate them into a quantitative assessment effort will still require extensive groundtruthing using visual or direct capture methods. Here we have examined the physical attributes of several dominant reef fish species found in the GOM and SEUS. Further, the results provided may help guide proper selection of acoustic frequencies for use within this species complex, in particular when resources may be limiting and only one or two frequencies available for implementation in a field study.

Funding

This work was supported by the Florida RESTORE Act Centers of Excellence Program (K.M.B. and W.F.P; 4701-1126-00-D); and the National Marine Fisheries Service Advanced Sampling Technology Work Group (K.M.B., J.C.T, G.P; NA15OAR4320064).

Acknowledgements

We thank the efforts by several laboratory personnel to assist with the field work and processing of these data, in particular, we thank, Benjamin Binder, Sarah Friedl, Miaya Galbach, Steve Garner, Nate Snyder, Allison White, and Aubree Zenone. Johnny Greene, Captain of Intimidator provided an efficient sampling platform and Brian Jones of the Dauphin Island Seaquarium provided housing for the fish prior to scanning. Additionally, we thank Cathy Cooper and Jennifer Yeager from the University of South Alabama Health University Hospital for assistance in the image acquisition and guidance for image processing. We appreciate comments from two anonymous reviewers for improving the manuscript. This is contribution #XXX from the Center for Coastal Oceans Research in the Institute of Water and Environment at Florida International University. This work was supported, in part, by a grant from the National Marine Fisheries Service Advanced Sampling Technology Working group and from the National Centers for Coastal Ocean Science. This work was completed under the guidance of the Florida International University IACUC protocol number: XXX.

References

Au, W. W., & Benoit-Bird, K. J. 2003. Acoustic backscattering by Hawaiian lutjanid snappers. II. Broadband temporal and spectral structure. The Journal of the Acoustical Society of America, 114 :2767-2774.

Bacheler, N. M., Schobernd, C. M., Schobernd, Z. H., Mitchell, W. A., Berrane, D. J., Kellison, G. T., & Reichert, M. J. 2013. Comparison of trap and underwater video gears for indexing reef fish presence and abundance in the southeast United States. Fisheries Research, 143, 81-88.

446 Benoit-Bird, K. J., Au, W. W., & Kelley, C. D. 2003. Acoustic backscattering by Hawaiian
447 lutjanid snappers. I. Target strength and swimbladder characteristics. The Journal of the
448 Acoustical Society of America, 114 :2757-2766.
449
450 Benoit-Bird, K. J., & Lawson, G. L. 2016. Ecological insights from pelagic habitats acquired
451 using active acoustic techniques. Annual review of marine science. 8:463-490.
452
453 Campbell, M.D., Pollack, A.G., Gledhill, C.T., Switzer, T.S. and DeVries, D.A., 2015.
454 Comparison of relative abundance indices calculated from two methods of generating video
455 count data. Fisheries Research, 170: 125-133.
456
457 Chandler-Wilde, S., Graham, I., Langdon, S., & Spence, E. 2012. Numerical-asymptotic
458 boundary integral methods in high-frequency acoustic scattering. Acta Numerica, 21, 89-305.
459
460 Clay, C.S., Horne, J.K., 1994. Acoustic models of fish: the Atlantic cod (*Gadus morhua*). Journal
461 of the Acoustical Society of America. 96, 1661–1668.
462
463 Cowan Jr., J.H., C.B. Grimes, W.F. Patterson III, C.J. Walters, A.C. Jones, W.J. Lindberg, D.J.
464 Sheehy, W.E. Pine III, J.E. Powers, M.D. Campbell, K.C. Lindeman, S.L. Diamond, R. Hilborn,
465 H.T. Gibson and K.A. Rose. 2011. Red snapper management in the Gulf of Mexico: science- or
466 faith-based? Reviews in Fish Biology and Fisheries 21:187-204.
467

Da Silva, R., Peloso, P. L. V., Sturaro, M. J., Veneza, I., Sampaio, I., Schneider, H. & Grazielle, G. 2018. Comparative analyses of species delimitation methods with molecular data in snappers (Perciformes: Lutjaninae). Mitochondrial DNA Part A 29: 1108–1114.

Die, D.J., V.R. Restrepo, J.M. Hoenig. 1988. Utility-per-recruit modeling: a neglected concept. Transactions of the American Fisheries Society 7:274-281.

Fässler, S. M., O'Donnell, C., & Jech, J. M. 2013. Boarfish (Capros aper) target strength modelled from magnetic resonance imaging (MRI) scans of its swimbladder. ICES Journal of Marine Science, 70:1451-1459.

Foote K.G., 1979, On representing the length dependence of acoustic target strengths of fish. J. Fish. Board Can. 36, 1490–1496.

Foote, K. G., 1980a. Importance of the swimbladder in acoustic scattering by fish: a comparison of gadoid and mackerel target strengths. The Journal of the Acoustical Society of America, 67:2084-2089.

Foote, K.G., 1980b. Effect of fish behaviour on echo energy: The need for measurements of orientation distributions. ICES Journal of Marine Science. 39:193–201.

Foote K.G., Francis D.T.I., 2002, Comparing Kirchhoff-approximation and boundary-element models for computing gadoid target strengths. Journal of the Acoustical Society of America. 111:1644–1654.

Forland, T.N., Hobæk, H. and Korneliussen, R.J., 2014. Scattering properties of Atlantic mackerel over a wide frequency range. ICES Journal of Marine Science, 71:1904-1912.

Forland, T.N., Hobæk, H., Ona, E. and Korneliussen, R.J., 2014. Broad bandwidth acoustic backscattering from sandeel—measurements and finite element simulations. ICES Journal of Marine Science, 71:1894-1903.

Francis, D. T. I., and Foote, K. G. 2003. Depth-dependent target strengths of gadoids by the boundary-element method. The Journal of the Acoustical Society of America, 114: 3136.

Furusawa, M., 1988. Prolate spheroidal models for predicting general trends of fish target strength. Journal of the Acoustical Society of Japan, 9:13-24.

Gastauer, S., Scoulding, B., Fässler, S.M., Benden, D.P. and Parsons, M., 2016. Target strength estimates of red emperor (Lutjanus sebae) with Bayesian parameter calibration. Aquatic Living Resources, 29:301.

510 Gastauer, S., Scoulding, B. and Parsons, M., 2017a. Towards acoustic monitoring of a mixed
511 demersal fishery based on commercial data: The case of the Northern Demersal Scalefish
512 Fishery (Western Australia). Fisheries Research, 195, pp.91-104.
513
514 Gastauer, S., Scoulding, B., Parsons, M. 2017b. Estimates of variability of goldband snapper
515 target strength and biomass in three fishing regions within the Northern Demersal Scalefish
516 Fishery (Western Australia). Fisheries Research 193: 250-262.
517
518 Gledhill, C. T., Lyczkowski-Shultz, J., Rademacher, K., Kargard, E., Crist, G., Grace, M. A.
519 1996. Evaluation of video and acoustic index methods for assessing reef-fish populations. ICES
520 Journal of Marine Science, 53:483-485.
521
522 Gold JR, Voelker G, Renshaw MA. 2011. Phylogenetic relationships of tropical western Atlantic
523 snappers in subfamily Lutjanidae (Lutjanidae: Perciformes) inferred from mitochondrial DNA
524 sequences. Biol J Linn Soc. 102:915–929.
525
526 Hazen, E. L., & Horne, J. K. 2003. A method for evaluating the effects of biological factors on
527 fish target strength. ICES Journal of Marine Science, 60:555-562.
528
529 Hilborn R., Walters C. J. Eds. 2013. Quantitative fisheries stock assessment: choice, dynamics
530 and uncertainty. Springer Science & Business Media, Dordrecht.
531

532 Holliday DV. 1977. The use of swimbladder resonance in the sizing of schooled pelagic fish.
533 Rapp. P.-V. Reun.- Cons. Int. Explor. Mer 170: 130-135.
534
535 Horne, J. K. 2003. The influence of ontogeny, physiology, and behaviour on the target strength
536 of walleye pollock (*Theragra chalcogramma*). ICES Journal of Marine Science, 60:1063–1074.
537
538 Jech, J. M., Horne, J. K., Chu, D., Demer, D. A., Francis, D. T. I., Gorska, N., Jones, B., Lavery,
539 A. C., Stanton, T. K., Macaulay, G.J., Reeder, D. B., and Sawada, K. 2016. Comparisons among
540 ten models of acoustic backscattering used in aquatic ecosystem research. Journal of the
541 Acoustical Society of America, 138: 3742–3764.
542
543 Jech, J. M., Lawson, G. L., Lavery, A. C., & Handling editor: David Demer. 2017. Wideband
544 (15–260 kHz) acoustic volume backscattering spectra of Northern krill (*Meganyctiphanes*
545 *norvegica*) and butterfish (*Peprilus triacanthus*). ICES Journal of Marine Science, 74:2249-
546 2261.
547
548 Johnston, S.V., Rivera, J.A., Rosario, A., Timko, M.A., Nealson, P.A. and Kumagai, K.K., 2006.
549 Hydroacoustic evaluation of spawning red hind (Epinephelus guttatus) aggregations along the
550 coast of Puerto Rico in 2002 and 2003.
551
552 Johnston, F.D., R. Arlinghaus, and U. Diekmann. 2010. Diversity and complexity of angler
553 behavior drive socially optimal input and output regulations in a bioeconomic recreational-
554 fisheries model. Canadian Journal of Fisheries and Aquatic Sciences. 67:1507-1531.

555

556 Love R.H., 1977, Target strength of an individual fish at any aspect. Journal of the Acoustical
557 Society of America. 62:1397–1403.

558

559 Lundgren, B. and Nielsen, J.R. 2008. A method for the possible species discrimination of
560 juvenile gadoids by broad band-width backscattering spectra vs. angle of incidence. ICES
561 Journal of Marine Science, 65:581-593.

562

563 Macaulay, G. J., Peña, H., Fässler, S. M. M., Pedersen, G., and Ona, E. 2013. Accuracy of the
564 Kirchhoff-Approximation and Kirchhoff-Ray-Mode Fish Swimbladder Acoustic Scattering
565 Models. PLoS ONE, 5(8), e64055.

566

567 MacLennan, D.N., 1990. Acoustical measurement of fish abundance. The Journal of the
568 Acoustical Society of America, 87: 1-15.

569

570 Nakken O., and K. Olsen. 1977. Target strength measurements of fish. Rapp. P. Reun. Cons. Int.
571 Explor. Met. 170:52-69.

572

573 Nesse, T. L., Hobæk, H., and Korneliussen, R. J. 2009. Measurements of acoustic-scattering
574 spectra from the whole and parts of Atlantic mackerel. ICES Journal of Marine Science, 66:
575 1169–1175.

576

577 Okumura, T., Masuya, T., Takao, Y., and Sawada, K. 2003. Acoustic scattering by an arbitrarily
578 shaped body: an application of the boundary-element method. ICES Journal of Marine Science,
579 60: 563–570.
580
581 Ona E., 1990, Physiological factors causing natural variations in acoustic target strength of fish.
582 J. Mar. Biol. Assoc. U. K. 70, 107–127.
583
584 Peña, H., & Foote, K. G. (2008). Modelling the target strength of *Trachurus symmetricus*
585 *murphyi* based on high-resolution swimbladder morphometry using an MRI scanner. ICES
586 Journal of Marine Science, 65(9), 1751-1761.
587
588 Reeder, D. B., Jech, J. M., and Stanton, T. K. 2004. Broadband acoustic backscatter and high-
589 resolution morphology of fish: Measurement and modeling. The Journal of the Acoustical
590 Society of America, 116:747-761.
591
592 Roa, C., K.M. Boswell, G. Pedersen, J.C. Taylor, and M. Bollinger. In review. Taxonomical
593 classification of reef fish based on a swim bladder BEM, broadband echosounder modeling; and
594 Bayesian, SVM, K-NN, and CNN estimators. Submitted to Journal of the Acoustical Society of
595 America.
596
597 Ross, T., Keister, J. E., & Lara-Lopez, A. 2013. On the use of high-frequency broadband sonar to
598 classify biological scattering layers from a cabled observatory in Saanich Inlet, British Columbia.
599 Methods in Oceanography, 5:19-38.

Rudershausen, P. J., Mitchell, W. A., Buckel, J. A., Williams, E. H., & Hazen, E. 2010. Developing a two-step fishery-independent design to estimate the relative abundance of deepwater reef fish: application to a marine protected area off the southeastern United States coast. Fisheries Research, 105:254-260.

Śmigaj, W., Arridge, S., Betcke, T., Phillips, J., and Schweiger, M. 2015. Solving Boundary Integral Problems with BEM++, ACM Transactions on mathematical software 6:1–6:40.

Scoulding, B., Chu, D., Ona, E., & Fernandes, P. G. 2015. Target strengths of two abundant mesopelagic fish species. The Journal of the Acoustical Society of America, 137:989-1000.

Simmonds, J. and MacLennan, D.N., 2005. *Fisheries acoustics: theory and practice*. John Wiley & Sons.

Stanton, T. K., Chu, D., & Wiebe, P. H. 1998. Sound scattering by several zooplankton groups. II. Scattering models. The Journal of the Acoustical Society of America, 103:236-253.

Stanton, T. K., Chu, D., Jech, J. M., and Irish, J. D. 2010. New broadband methods for resonance classification and high-resolution imagery of fish with swimbladders using a modified commercial broadband echosounder. ICES Journal of Marine Science, 67: 365–378.

622 Stanton, T. K., Sellers, C. J., & Jech, J. M. 2012. Resonance classification of mixed assemblages
623 of fish with swimbladders using a modified commercial broadband acoustic echosounder at 1–6
624 kHz. Canadian Journal of Fisheries and Aquatic Sciences, 69:854-868.
625
626 Zakharia, M. E., Magand, F., Hetroit, F., & Diner, N. 1996. Wideband sounder for fish species
627 identification at sea. ICES Journal of Marine Science, 53:203-2.
628

Figure and Table Captions

Figure 1. Morphological variations of swim bladders of reef associated species: A) blue striped grunt; B) gray triggerfish; C) hogfish; D) red band parrotfish; E) red snapper; F) tomtate; G) vermillion snapper; and H) white grunt.

Figure 2. Example CT scan of a red snapper illustrating the morphological metrics derived from each individual: total length (a), fish width (b), fish thickness (c), bladder angle (d), bladder length (e), bladder height (f).

Figure 3. Principal components analysis of fish and bladder metrics by species (colored symbols). Error bars represent standard error of PC1 and PC2 for each species. Component loadings are displayed as rays to each modeled variable. See Table S1 for abbreviated common names of species; scientific names appear in the text.

Figure. 4. Significant positive log-linear relationship ($y = -0.52 + 0.74log_{10}(Fish\_Length)$; $F_{1,137}=398.2$, $p<0.001$, $R^2=0.80$) between measured fish length (total length cm) and measured bladder length (cm) for each individual CT scan. Species are identified by colored symbols. Summary statistics of morphological variables for each species and species abbreviations can be found in Table S1.

Figure 5. Target strength ([dB re $1m^2$] colormap) responses of individual reef fish species. A) bank sea bass; B) blue striped grunt; C) gray triggerfish; D) hogfish; E) red band parrotfish; F) red snapper; G) tomtate; H) vermilion snapper; and I) white grunt.

652

653 Figure 6. Species specific averaged σ_{bs} response (m^2) with 95% confidence intervals (broken
654 lines) around the mean (solid line). Vertical reference lines represent nominal operating
655 frequencies in fisheries acoustics (38, 70, 120, and 200 kHz).

656

657 Figure 7. The model derived intercepts (b_0 and b_{20}) for the target strength-length regression for
658 all species with greater than four individuals.

659

660 Figure 8. Kernel density distribution of target strength (TS [dB re $1m^2$]) for each species with
661 greater than 4 individuals, representing response from +/-10 degrees from normal orientation
662 across all frequencies (30-200 kHz).

663

664 Table 1. Summary statistics of bladder metrics manually measured from individual CT images.
665 Means (+/- standard errors) are provided. Fish Length/Bladder Length and Fish Height/Bladder
666 Height are ratios derived from manual measurements.

667

668 Table 2. Regression model fits for fish length (cm) and swimbladder length (cm) relationships
669 among all species that had four or greater individuals.

670

671 Table 3. Target Strength (dB re $1m^2$) - Fish Length (cm) regression coefficients fitted to modeled
672 species with at least four individuals (see Table S1). Model coefficients (slope, m; intercept, b_0;
673 and b_{20} intercept) and coefficients of determination (r^2_{b0} and r^2_{b20}) are provided. Regression
674 models where the slope was fixed (m = 20) have intercept values reported as (b_{20}).

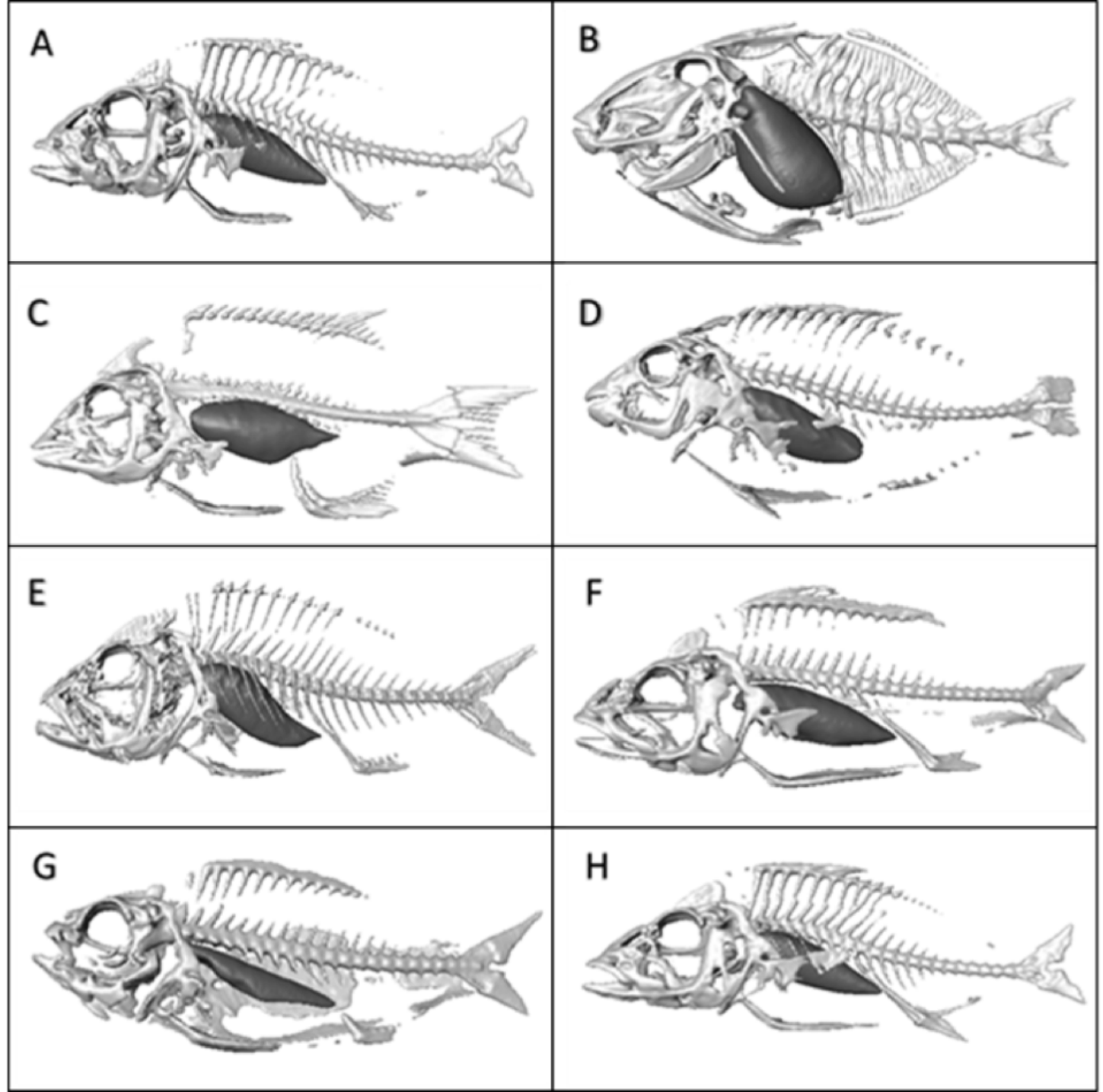
A
B
C
D
E
F
G
H

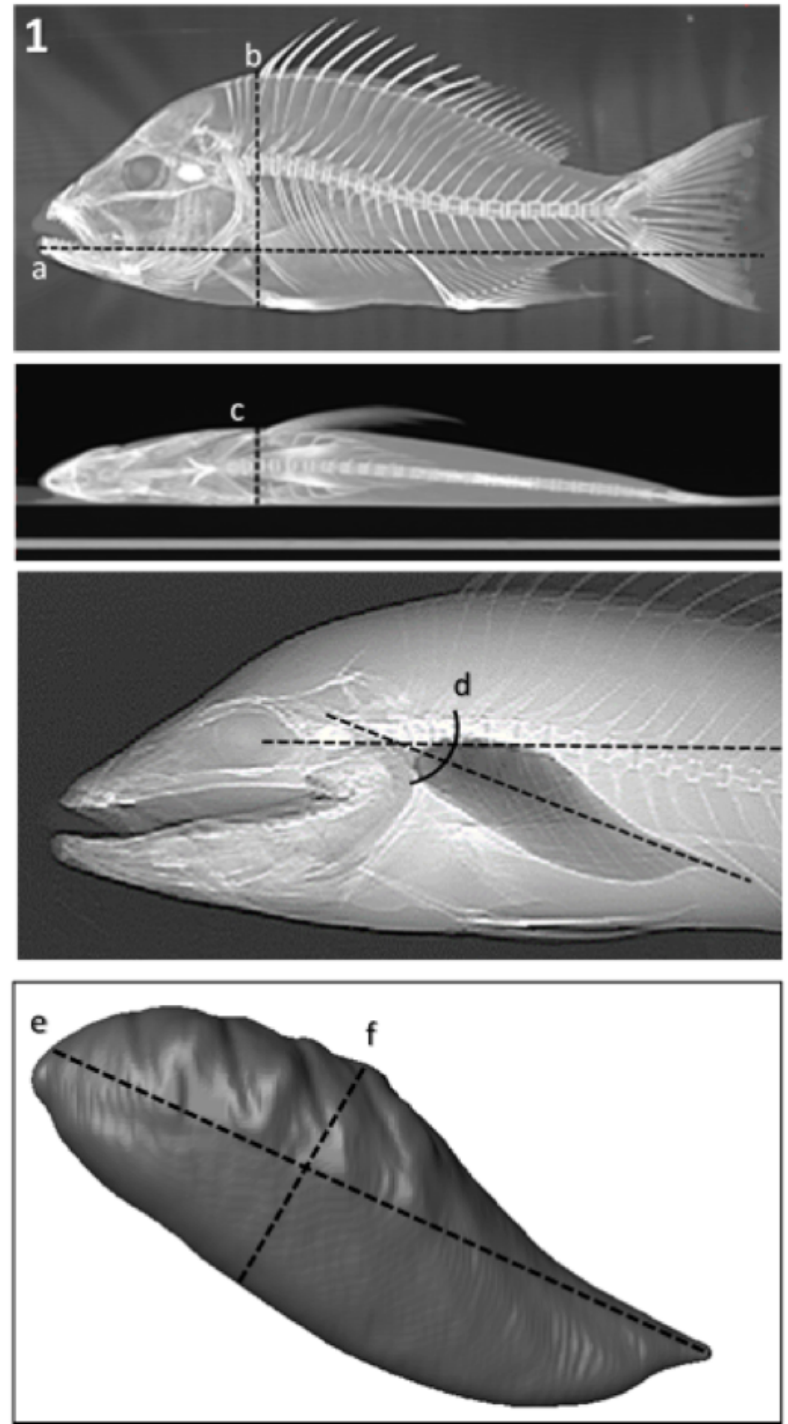
1
b
a
c
d
e
f

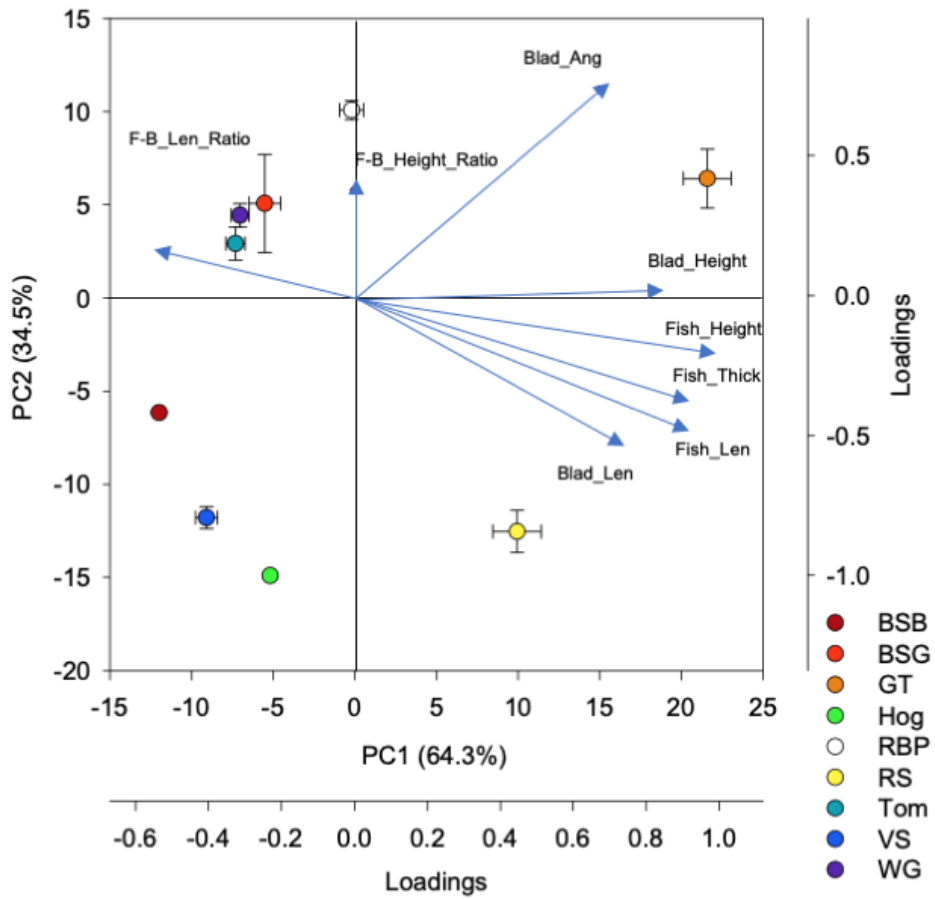
Blad_Ang
F-B_Len_Ratio
F-B_Height_Ratio
Blad_Height
Fish_Height
Fish_Thick
Fish_Len
Blad_Len
PC2 (34.5%)
PC1 (64.3%)
Loadings
Loadings
BSB
BSG
GT
Hog
RBP
RS
Tom
VS
WG

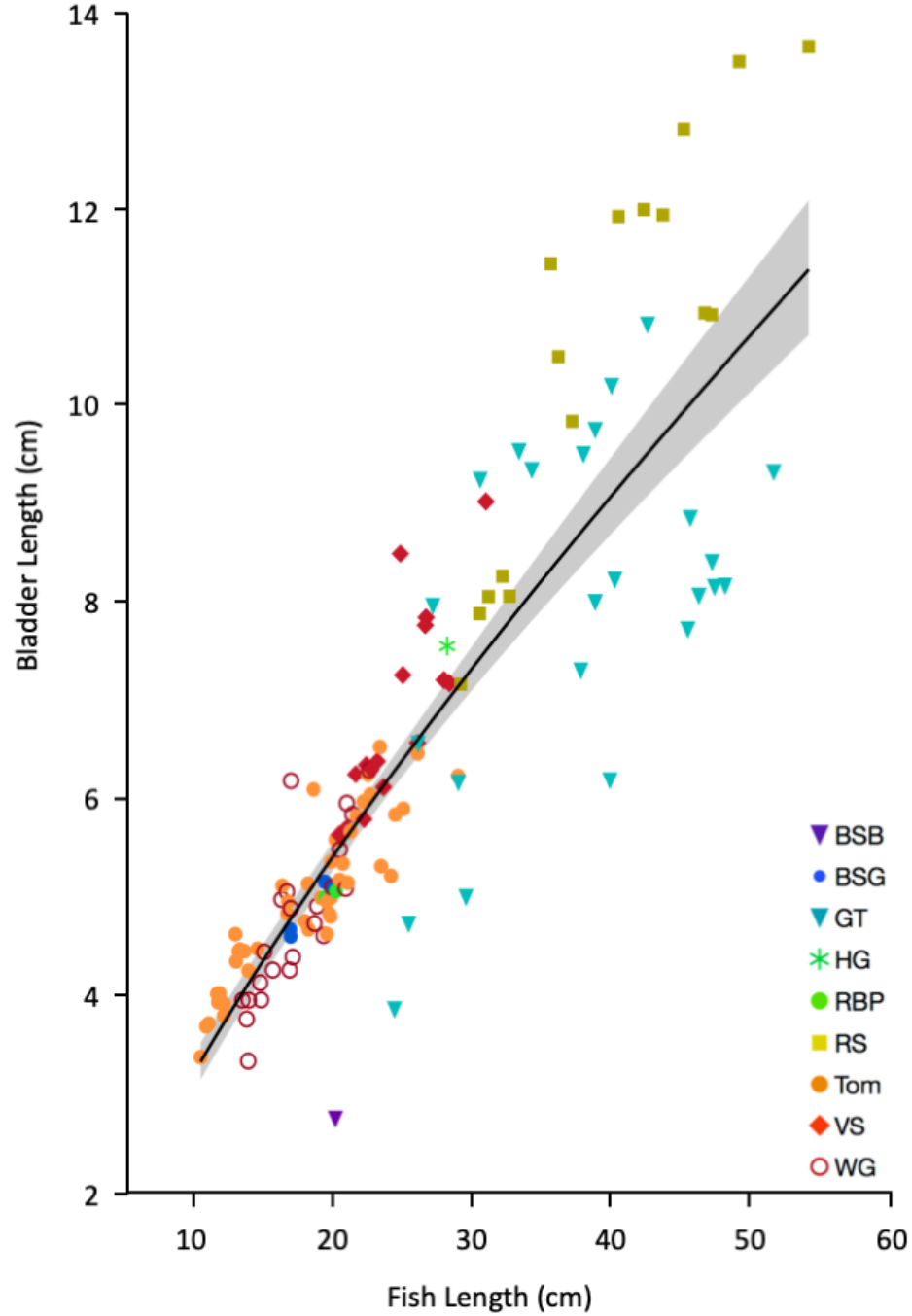
Bladder Length (cm)
Fish Length (cm)
14
12
10
8
6
4
2
10
20
30
40
50
60
BSB
BSG
GT
HG
RBP
RS
Tom
VS
WG

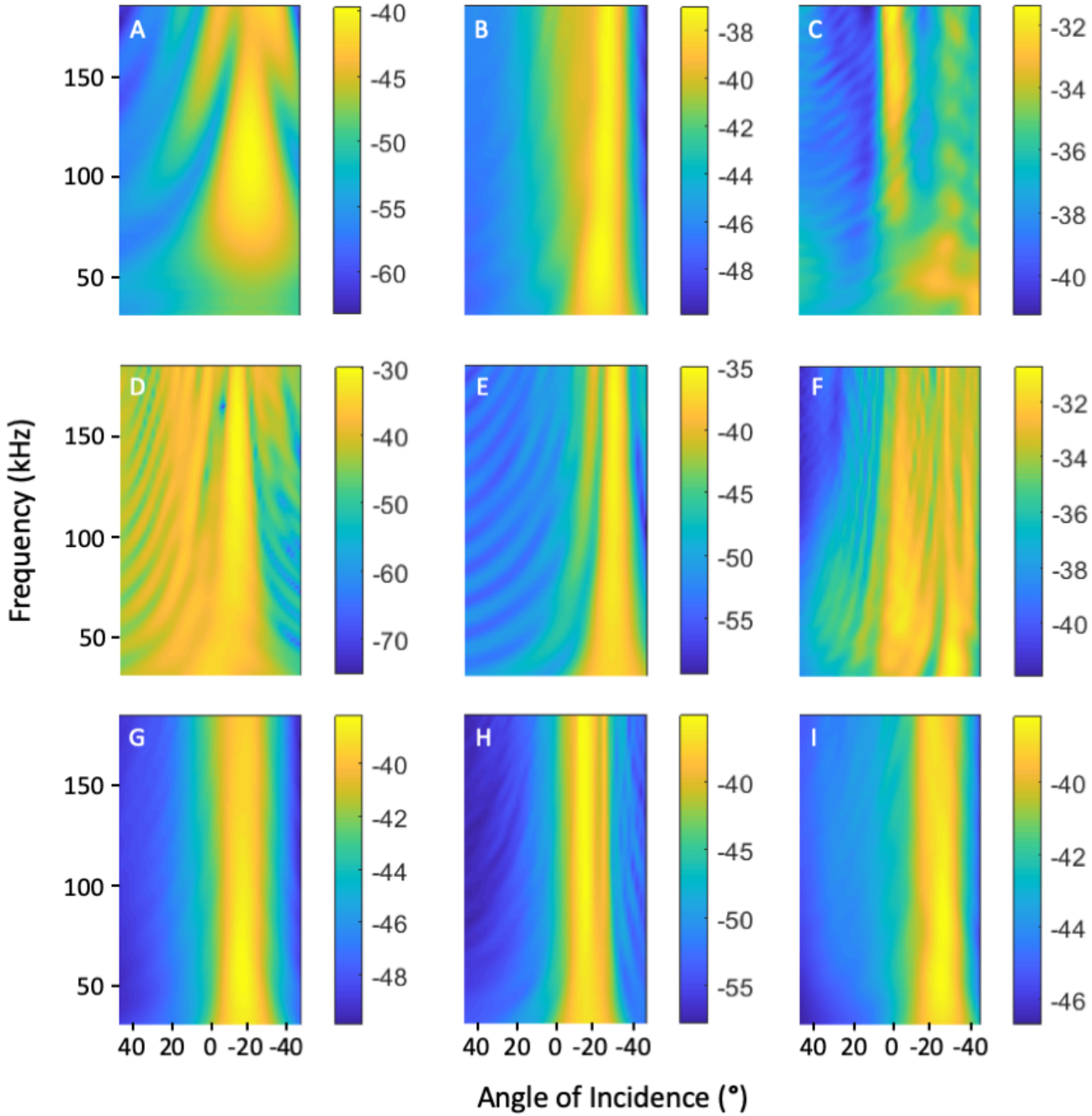
A
B
C
D
E
F
G
H
I
150
100
50
-40
-45
-50
-55
-60
-38
-40
-42
-44
-46
-48
-32
-34
-36
-38
-40
-30
-40
-50
-60
-70
-35
-40
-45
-50
-55
-32
-34
-36
-38
-40
-40
-42
-44
-46
-48
-40
-45
-50
-55
-40
-42
-44
-46
40 20 0 -20 -40
Frequency (kHz)
Angle of Incidence (°)

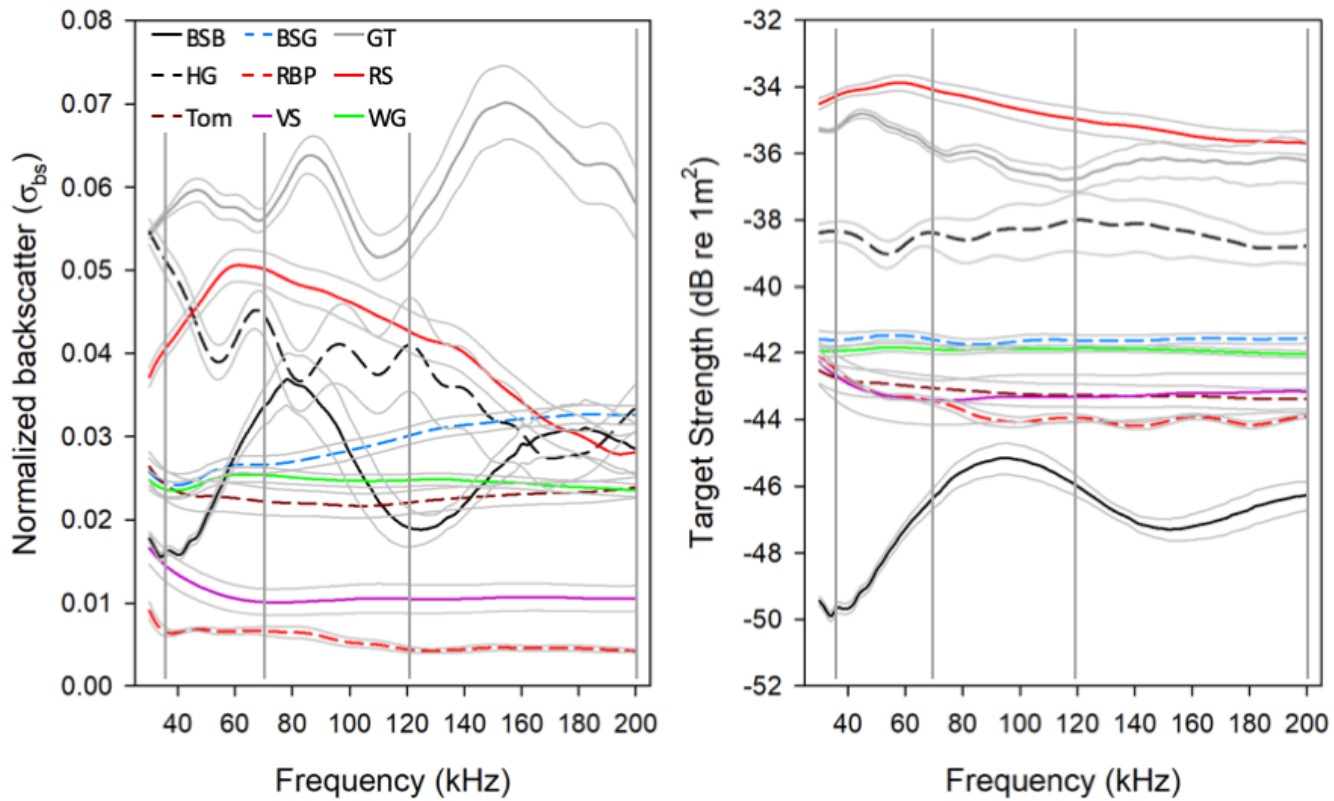
BSB
BSG
GT
HG
RBP
RS
Tom
VS
WG
Normalized backscatter (σ_{bs})
0.08
0.07
0.06
0.05
0.04
0.03
0.02
0.01
0.00
40 60 80 100 120 140 160 180 200
Frequency (kHz)
Target Strength (dB re 1m^2)
-32
-34
-36
-38
-40
-42
-44
-46
-48
-50
-52
40 60 80 100 120 140 160 180 200
Frequency (kHz)

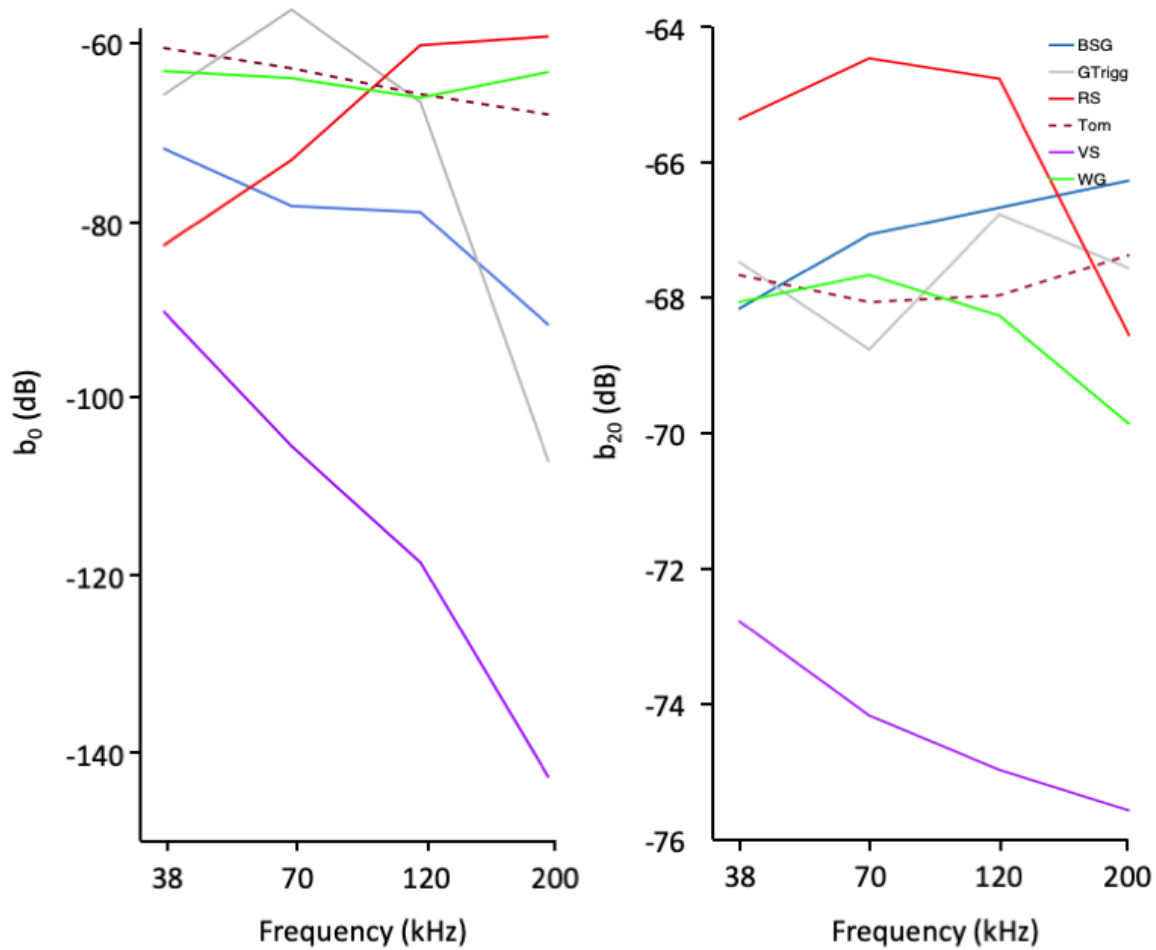
-60
-80
-100
-120
-140
b_0 (dB)
38
70
120
200
Frequency (kHz)
-64
-66
-68
-70
-72
-74
-76
b_{20} (dB)
BSG
GTrigg
RS
Tom
VS
WG
38
70
120
200
Frequency (kHz)

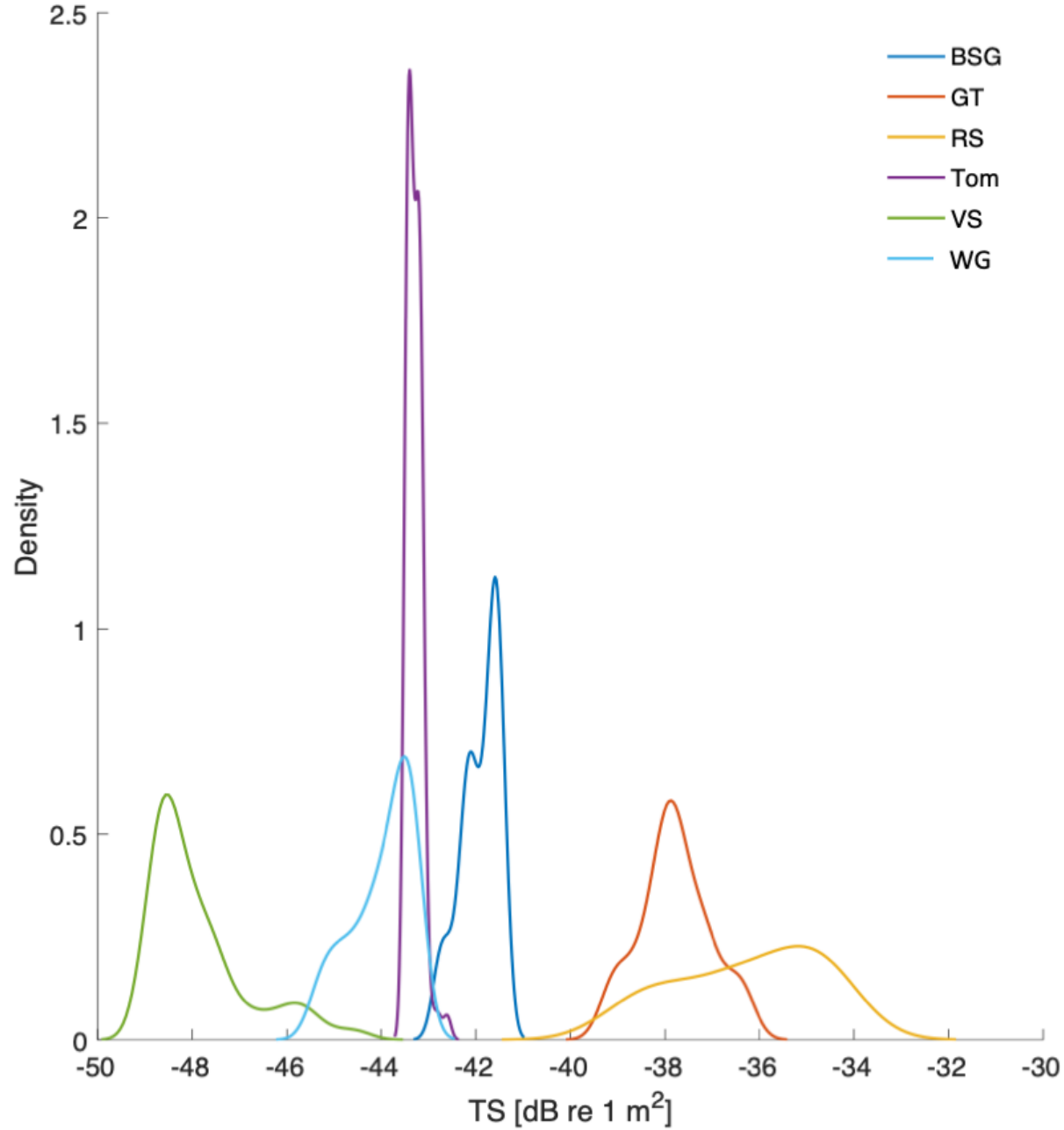
2.5
2
1.5
1
0.5
0
Density
-50
-48
-46
-44
-42
-40
-38
-36
-34
-32
-30
TS [dB re 1 m^2]
BSG
GT
RS
Tom
VS
WG

Table 1. Summary statistics of bladder metrics manually measured from individual CT images. Means (+/- standard errors) are provided. Fish Length/Bladder Length and Fish Height/Bladder Height are ratios derived from manual measurements.

Species	n	Bladder height (mm)	Bladder length (mm)	Bladder angle (deg)	Fish length (mm)	Fish height (mm)	Fish thickness (mm)	Ratio: bladder length/ fish length	Ratio: bladder height/ fish height
Bank sea bass (BSB)	1	0.77 (-)	2.75 (-)	19.98 (-)	20.0 (-)	4. 36 (-)	3.12 (-)	0.14 (-)	0.18 (-)
Blue striped grunt (BSG)	4	1.58 (0.12)	4.87 (0.14)	32.8 (2.69)	18.12 (0.80)	6.13 (0.18)	2.44 (0.06)	0.27 (0.01)	0.26 (0.01)
Gray triggerfish (GT)	26	3.54 (0.29)	8.04 (0.36)	49.27 (1.31)	37.68 (1.59)	15.09 (0.55)	5.35 (0.21)	0.22 (0.01)	0.24 (0.02)
Hogfish (Hog)	1	2.72 (-)	7.54 (-)	16.1 (-)	28.04 (-)	10.74 (-)	3.96 (-)	0.27 (-)	0.25 (-)
Red band parrotfish (RBP)	2	1.77 (0.03)	5.02 (0.03)	39.95 (0.85)	19.66 (0.37)	6.81 (0.02)	2.34 (0.22)	0.26 (0.003)	0.26 (0.004
Red Snapper (RS)	23	2.18 (0.27)	9.96 (0.62)	26.83 (0.49)	39.26 (1.69)	11.95 (0.45)	5.19 (0.20)	0.25 (0.01)	0.18 (0.02)
Tomtate (Tom)	50	1.29 (0.14)	5.03 (0.13)	30.18 (0.78)	18.19 (0.66)	5.27 (0.18)	2.21 (0.09)	0.29 (0.01)	0.25 (0.02)
Vermillion snapper (VS)	18	1.02 (0.09)	6.86 (0.25)	16.9 (0.40)	24.44 (0.75)	6.62 (0.22)	2.92 (0.12)	0.28 (0.01)	0.15 (0.01)
White grunt (WG)	24	1.53 (0.06)	4.76 (0.17)	31.40 (0.53)	17.19 (0.58)	6.15 (0.24)	2.22 (0.08)	0.28 (0.01)	0.25 (0.004)

Table 2. Regression model fits for fish length (cm) and swimbladder length (cm) relationships among all species that had four of greater individuals.

Species	Model	R^2	P
Blue striped grunt	$Log_{10}(Bladder\_Length) = -0.27 + 0.64 * Log_{10}(Fish\_Length)$	0.95	0.027
Gray triggerfish	$Log_{10}(Bladder\_Length) = -0.48 + 0.70 * Log_{10}(Fish\_Length)$	0.38	0.001
Red snapper	$Log_{10}(Bladder\_Length) = -1.27 + 0.99 * Log_{10}(Fish\_Length)$	0.82	<0.001
Tomtate	$Log_{10}(Bladder\_Length) = -0.04 + 0.54 * Log_{10}(Fish\_Length)$	0.84	<0.001
Vermilion snapper	$Log_{10}(Bladder\_Length) = -1.27 + 0.99 * Log_{10}(Fish\_Length)$	0.71	<0.001
White grunt	$Log_{10}(Bladder\_Length) = -0.90 + 0.86 * Log_{10}(Fish\_Length)$	0.70	<0.001

Table 3. Target Strength (dB re $1m^2$) - Fish Length (cm) regression coefficients fitted to modeled species with at least four individuals (see Table S1). Model coefficients (slope, m; intercept, b_0; and b_{20} intercept) and coefficients of determination (r^2_{b0} and r^2_{b20}) are provided. Regression models where the slope was fixed (m = 20) have intercept values reported as (b_{20}).

	38 kHz				**70 kHz**					**120 kHz**			**200 kHz**			
Species	***m***	***b*$_0$**	***b*$_{20}$**	***r*$^2_{b0}$/*r*$^2_{b20}$**	***m***	***b*$_0$**	***b*$_{20}$**	***r*$^2_{b0}$/ *r*$^2_{b20}$**	***m***	***b*$_0$**	***b*$_{20}$**	***r*$^2_{b0}$/ *r*$^2_{b20}$**	***m***	***b*$_0$**	***b*$_{20}$**	***r*$^2_{b0}$/ *r*$^2_{b20}$**
Blue striped grunt	22.9	-71.9	-68.2	0.39/0.38	28.9	-78.4	-67.1	0.69/0.62	29.8	-79.1	-66.7	0.70/0.62	40.3	-91.9	-66.3	0.53/0.39
Gray triggerfish	19.0	-65.9	-67.5	0.30/0.30	11.9	-56.3	-68.8	0.05/0.03	19.9	-66.7	-66.8	0.31/0.30	45.6	-107.3	-67.6	0.45/0.31
Red snapper	31.4	-82.9	-65.4	0.93/0.81	25.6	-73.2	-64.5	0.77/0.73	17.1	-60.3	-64.8	0.41/0.40	14.0	-59.3	-68.6	0.20/0.17
Tomtate	14.3	-60.6	-67.7	0.50/0.42	15.8	-62.9	-68.1	0.50/0.53	18.2	-65.8	-68.0	0.65/0.65	20.6	-68.1	-67.4	0.65/0.66
Vermillion snapper	32.7	-90.3	-72.8	0.16/0.13	42.7	-105.5	-74.2	0.30/0.22	51.7	-118.6	-75.0	0.28/0.17	68.9	-142.9	-75.6	0.29/0.14
White grunt	16.0	-63.2	-68.1	0.24/0.23	16.9	-64.0	-67.7	0.27/0.26	18.3	-66.2	-68.3	0.16/0.16	14.65	-63.3	-69.9	0.05/0.04